Simultaneous B_1 and T_1 Mapping Using Spiral Multislice Variable Flip Angle Acquisitions for Whole-Brain Coverage in Less Than One Minute

Rahel Heule[1,2,3], Josef Pfeuffer[4], Craig H. Meyer[5], and Oliver Bieri[1,2]

[1]Division of Radiological Physics, Department of Radiology, University Hospital Basel, University of Basel, Basel, Switzerland.
[2]Department of Biomedical Engineering, University of Basel, Basel, Switzerland.
[3]High Field Magnetic Resonance, Max Planck Institute for Biological Cybernetics, Tübingen, Germany.
[4]Siemens Healthcare, Application Development, Erlangen, Germany.
[5]Department of Biomedical Engineering, University of Virginia, Charlottesville, VA, USA.

Published in ***Magnetic Resonance in Medicine*** as a ***full paper***.

Word count: 200 (Abstract), 5800 (Body), 9 Figures, 1 Table, 27 References.

Correspondence to:
Rahel Heule, PhD
High Field Magnetic Resonance
Max Planck Institute for Biological Cybernetics
Max-Planck-Ring 11
72076 Tübingen, Germany
Email: rahel.heule@tuebingen.mpg.de
Phone: +49-7071-601-704
Fax: +49-7071-601-702

Running title: Simultaneous B_1 and T_1 Mapping Using Spiral Multislice VFA Acquisitions.

ABSTRACT

Purpose: Variable flip angle (VFA)-based T_1 quantification techniques are highly sensitive to B_1 inhomogeneities and to residual T_2 dependency arising from incomplete spoiling. Here, a rapid spiral VFA acquisition scheme with high spoiling efficiency is proposed for simultaneous whole-brain B_1 and T_1 mapping.

Methods: VFA acquisitions at two different flip angles are performed to quantify T_1 using a steady-state prepared spiral 2D multislice spoiled gradient-echo sequence with the acquisition of 10 and 20 spiral interleaves at 1.5 T and 3 T, respectively. Additionally, parallel imaging acceleration of factor 2 is investigated at 3 T. The free induction decay induced by the preparation pulse is sampled by a single-shot spiral readout to quantify B_1.

Results: The *in vitro* and *in vivo* validations yielded good agreement between the derived spiral VFA B_1 and the acquired reference B_1 maps as well as between the B_1-corrected spiral VFA T_1 and the reference T_1 maps. The spiral VFA acquisitions in the human brain delivered artifact-free B_1 and T_1 maps and demonstrated high reproducibility at 1.5 T and 3 T.

Conclusion: Reliable simultaneous spiral VFA B_1 and T_1 quantification was feasible with acquisition times of less than one minute for whole-brain coverage at clinically relevant resolution.

Keywords (3-6): B_1; T_1; variable flip angle (VFA); spiral trajectories; steady-state preparation; whole-brain coverage.

INTRODUCTION

Snapshot-like mapping of magnetic resonance parameters with high accuracy has been a long-standing goal in the field of quantitative MRI. Relaxation is the most fundamental mechanism governing the magnetic resonance signal level and soft tissue contrast. Mapping of proton relaxation times directly reflects the biophysical properties of tissues at a molecular level. In a clinical context, quantification of longitudinal (T_1) and transverse (T_2, T_2*) relaxation times has the potential to provide better tissue discrimination and thus improved detection of pathological tissue changes compared to conventional weighted magnetic resonance imaging. The biological correlates of MR relaxation times have been widely investigated, especially in the field of the clinical neurosciences (1).

There exist many clinical and research studies focused on the development and evaluation of relaxation time mapping techniques for human brain tissue characterization. However, a literature search reveals that in particular for the longitudinal relaxation parameter T_1, to date, no reliable reference values are available. Reported white matter T_1 values measured in the human brain at 3 Tesla using three common techniques – inversion recovery (IR) (2,3), Look-Locker (LL) (4,5), and variable flip angle (VFA) (6) – range from 690 to 1100 ms as pointed out in a recent comparative study (7). Surprisingly, even the IR method often referred to as gold standard delivers brain white matter values which vary by 50% in the literature (cf. Ref. (7), Table 1). A standardized IR protocol and T_1 fitting procedure was developed to eliminate this variation suggesting single-slice imaging with non-selective inversion, sampling the signal at four time points, and fitting the complex data with five free parameters (8). While, by this means, robust and accurate T_1 values can be obtained, the required total scan time becomes prohibitively long.

Besides accuracy, acquisition speed is essential for clinical applicability. LL and VFA techniques allow faster imaging and volumetric coverage (9,10); however, they show a distinct sensitivity to flip angle miscalibrations as typically resulting from radiofrequency (RF) transmit field (B_1) inhomogeneities and to incomplete spoiling (i.e. to residual T_2 dependency). These two factors were identified as the possible sources causing the large variability in reported T_1 values (7,11).

Recently, an interleaved 2D multislice spoiled gradient echo (SPGR) sequence with high spoiling efficiency because of long-TR and gradient spoiling, thus guaranteeing complete elimination of transverse coherences, was suggested for T_2-bias-free VFA T_1 quantification with whole-brain coverage (12). In Ref. (13), it was demonstrated that 2D multislice SPGR imaging can be accelerated significantly by a 2D spiral readout while still yielding highly accurate T_1 values. In the respective study, the transition to steady state was minimized by an optimized steady-state preparation module consisting of a single preparation pulse preceding the actual SPGR image acquisition. To correct flip angle miscalibrations, VFA T_1 mapping techniques typically require an additional B_1 mapping scan that, however, prolongs the overall measurement time (7,11-14).

In this work, a rapid simultaneous B_1 and T_1 quantification technique is suggested using steady-state prepared spiral multislice VFA imaging similarly to Ref. (13) but without an additional calibration measurement for B_1 estimation, thus saving scan time. For simultaneous B_1 mapping, the free induction decay (FID) signal generated by the applied single preparation pulse is acquired with a single-shot spiral readout. As a result, reliable whole-brain T_1 quantification without any T_2 or B_1 bias proves to be feasible in an overall scan time of less than one minute at field strengths of 1.5 T and 3 T. The simultaneous B_1 and T_1 mapping method is validated *in vitro* in a manganese-doped aqueous probe (0.125 mM $MnCl_2$ in H_2O) as well as *in vivo* in the human brain.

METHODS

The postprocessing of the acquired MR data and the visualization of the results were done using Matlab R2017a (The MathWorks, Inc., Natick, MA). The MR scans were performed at 1.5 T (Magnetom Avanto fit, Siemens Healthcare, Erlangen, Germany) as well as at 3 T (Magnetom Prisma, Siemens Healthcare, Erlangen, Germany), in both cases with the standard 20-channel receive head coil of the manufacturer. The *in vivo* human brain MR measurements were approved by the local ethics committee.

Spiral VFA acquisition scheme

To simultaneously quantify B_1 and T_1, the acquisition strategy suggested in Ref. (13) for T_1 mapping was revised for the acquisition of four instead of two contrasts without any scan

time prolongation (cf. Fig. 1). The k-space of all four contrasts was sampled according to a 2D constant-density spiral-out trajectory (15) at a receive bandwidth of 400 kHz. The acquired data was reconstructed with an iterative non-Cartesian self-consistent parallel imaging reconstruction (SPIRiT (16)) using an auto-stop criterion, also in case the k-space was fully sampled at the Nyquist rate, to implicitly derive the optimal density compensation function for the gridding algorithm. The spiral trajectory was calibrated in a one-time process using the Tan-Meyer eddy current model (17). All data processing was performed in the image domain after SPIRiT reconstruction and coil combination. Adaptive combine was selected as coil combine mode as supplied by the standard vendor's processing pipeline.

In complete analogy to Ref. (13), the two contrasts needed for T_1 quantification were acquired using a prototype interleaved 2D multislice SPGR sequence with a spiral readout and a steady-state preparation scheme, repeated at two different nominal flip angles ($\alpha_{nom,1}$ = 17° and $\alpha_{nom,2}$ = 80°). A relatively long TR of 250 ms was used and in each TR, 11 slices were excited in an interleaved manner, separated by a center-to-center spacing of 15 mm (i.e. five times the slice thickness) to mitigate slice crosstalk and magnetization-transfer-related effects. As illustrated in Figure 1a, the excitation of multiple slices within TR leads to the accumulation of a large spoiler gradient area per TR (A_G); in this work, A_G = 459 (mT/m)·ms (≈ 11 · 41.7 (mT/m)·ms). Because of the combined influence of the long repetition time and diffusion spoiling (induced by the large spoiler gradient moment), the SPGR sequence depicted in Figure 1 is characterized by an extremely high spoiling efficiency (12,13). Consequently, the acquired steady-state signal can be considered to be ideally spoiled and thus governed by the Ernst equation (18).

At 1.5 T, the 2D multislice SPGR acquisitions were performed with 10 spiral interleaves resulting in a readout time of 10.7 ms. At 3 T, the number of interleaves was increased to 20 and the number of sampling points per spiral interleave reduced, shortening the readout time to 6.6 ms and consequently reducing off-resonance sensitivity. The receive bandwidth (= 400 kHz) and thus the dwell time were not changed. A short scan time of 2.5 s and 5 s was achieved at 1.5 T and 3 T, respectively, to acquire one slice group consisting of 11 slices with an in-plane resolution of 1.3 x 1.3 mm^2 (field-of-view: 256 x 256 mm^2) and a slice thickness of 3 mm. In addition, at 3 T, the performance of SPIRiT with an acceleration factor of R = 2

was investigated leading to scan times that were identical to the acquisitions at 1.5 T (i.e., 2.5 s per slice group).

Because of the short scan time per slice group, effective steady state preparation was crucial to avoid any potential bias in the T_1 quantification due to non-steady-state conditions during the beginning of the image acquisition (cf. Ref. (13)). The transition to steady state was minimized by a single preparation pulse with nominal flip angle β_{nom} and recovery period T_{rec} ($\geq$ TR) preceding the imaging module (cf. Fig. 1a). The parameters β_{nom} and T_{rec} were optimized for tissue T_1 and T_2 depending on the imaging module parameters (i.e., TR and α_{nom}). The following optimal settings were used as derived in Ref. (13): $\beta_{nom,1} = 34°$ / $T_{rec,1} = 250$ ms for the low-flip-angle acquisition ($\alpha_{nom,1} = 17°$) and $\beta_{nom,2} = 102°$ / $T_{rec,2} = 350$ ms for the high-flip-angle acquisition ($\alpha_{nom,2} = 80°$). Including the preparation time, the effective scan time per slice group was 2.75 s / 2.85 s for $\alpha_{nom,1}$ / $\alpha_{nom,2}$ at 1.5 T with R = 1 and 3 T with R = 2 and 5.25 s / 5.35 s at 3 T with R = 1.

While in Ref. (13), the preparation module was solely used for steady-state preparation, in this work, the free induction decay (FID) signal induced by the preparation pulse was sampled with an in-plane resolution of 5.3 x 5.3 mm^2 by a single-shot spiral trajectory with a readout time of 12.4 ms and 12.1 ms at 1.5 T and 3 T, respectively. By this means, two low-resolution contrasts originating from the FIDs that are created by the low-flip-angle ($\beta_{nom,1} = 34°$) and high-flip-angle ($\beta_{nom,2} = 102°$) preparation pulses can be obtained suited for B_1 mapping. Apart from the in-plane resolution, the geometry settings of the two contrasts acquired for B_1 mapping and the two contrasts acquired for T_1 mapping were the same (identical field-of-view, slice thickness, slice positioning, and number of slices per slice group), cf. Figure 1. All four contrasts were acquired at the same echo times: TE = 3.5 ms and TE = 3.7 ms at 1.5 T and 3 T, respectively.

To obtain whole-brain coverage, five slice groups, each consisting of 11 slices, were measured with interleaved positioning (i.e., in total 55 slices, cf. Fig. 1b). Overall scan time for the acquisition of the four contrasts was 28 s at 1.5 T with R = 1 / 3 T with R = 2 and 53 s at 3 T with R = 1. Since the scan time per slice group was only of the order of seconds, it was essential to ensure that the slices of consecutively acquired slice groups were not adjacent to avoid slice crosstalk impairment on the signal amplitudes (cf. Fig. 1b). The five slice groups

were first all measured at low flip angle ($\beta_{nom,1}$ / $\alpha_{nom,1}$) and then at high flip angle ($\beta_{nom,2}$ / $\alpha_{nom,2}$). The time interval from the acquisition end of a given slice group at low flip angle to its re-excitation at high flip angle was at least ≈ 11 s; thus sufficiently long to allow full T_1 recovery of the magnetization for the whole range of T_1 values encountered in human brain tissues at 1.5 T and 3 T.

VFA B_1 and T_1 calculation

Since a 2D acquisition strategy was used, the effect of the non-rectangular slice profile had to be considered. For slice selection during both the preparation as well as the imaging module, Hanning-windowed apodized SINC pulses with a time-bandwidth-product of 8 and a duration of 3840 µs were applied. Based on Bloch simulations, the response of the transverse magnetization to the applied RF pulse was calculated for N = 200 discrete samples across the slice. An actual flip angle at the center of the slice profile of $\beta_{act} = c_{B1} \cdot \beta_{nom}$ and $\alpha_{act} = c_{B1} \cdot \alpha_{nom}$ was assumed for the preparation and imaging pulses, respectively (c_{B1}: B_1 scaling factor to account for flip angle miscalibrations caused by transmit field inhomogeneities). Since c_{B1} and thus β_{act} / α_{act} are not known a priori, a lookup table was created for a whole actual flip angle range (from 0.1° to 180° in steps of 0.1°), containing the respective slice profiles, i.e., the flip angle and phase distributions of the transverse magnetization across the slice.

The x (real) and y (imaginary) components of the FID sampled during the preparation module were then derived by a discrete summation over the slice profile as

$$S_{\beta,x} = K \cdot \sum_{i=1}^{N} \sin \beta_i \cos \theta_i \quad [1]$$

and

$$S_{\beta,y} = K \cdot \sum_{i=1}^{N} \sin \beta_i \sin \theta_i \quad [2]$$

with a total signal amplitude of

$$S_\beta = \sqrt{S_{\beta,x}{}^2 + S_{\beta,y}{}^2}. \quad [3]$$

In Equations [1] and [2], the factor K reflects the proton density, coil sensitivity, and T_2^* relaxation; β_i and θ_i represent the flip angle and phase, respectively, at the location i across the slice calculated for $\beta_{act} = c_{B1} \cdot \beta_{nom}$. The signal ratio $s_\beta = S_{\beta 1}/S_{\beta 2}$ depends thus only on a single unknown parameter, the B_1 scaling factor c_{B1}, while the proportionality factor K cancels out. Based on a numerical minimization algorithm – here a golden section search (19)

with a search interval that is limited by an upper guess of $c_{B1,u} = 2$ – an estimate for c_{B1} can be derived as

$$c_{B1} = \arg\min\{c_{B1} \in [0, c_{B1,u}]: |s_{\beta,meas} - s_{\beta,calc}(c_{B1})|\} \quad [4]$$

where $s_{\beta,meas}$ denotes the signal ratio obtained from the measured signal amplitudes and $s_{\beta,calc}$ the ratio calculated based on Equations [1] to [3]. In a last step, the obtained B_1 ($\equiv c_{B1}$) maps were processed by 3D median filtering along the three spatial dimensions with kernel sizes of [11 11 3] and [19 19 7] in [x = read y = phase z = slice] encoding direction for the *in vitro* and *in vivo* data, respectively. The B_1 maps were not masked, in particular not skull-stripped in the *in vivo* case, prior to filtering to avoid introducing a bias at the edges of the brain. A median filter was chosen since apart from smoothing it is suited to remove any spatial bias in regions where the whole-brain B_1 mapping may be inaccurate as in the ventricles or failed due to signal voids as in the skull.

Similarly, T_1 was derived based on the signal ratio $s_\alpha = S_{\alpha1}/S_{\alpha2}$ where $S_{\alpha1}$ and $S_{\alpha2}$ are ideally spoiled steady-state signal amplitudes referring to the acquisitions with $\alpha_{nom,1}$ and $\alpha_{nom,2}$, respectively, and can be calculated by summing over the slice profile (cf., Refs. (12,20)):

$$S_\alpha = \sqrt{{S_{\alpha,x}}^2 + {S_{\alpha,y}}^2} \quad [5]$$

with

$$S_{\alpha,x} = K \cdot \sum_{i=1}^{N} S_{ideal}(T_1, TR, \alpha_i) \cdot \cos\theta_i \quad [6]$$

and

$$S_{\alpha,y} = K \cdot \sum_{i=1}^{N} S_{ideal}(T_1, TR, \alpha_i) \cdot \sin\theta_i \quad [7]$$

In Equations [6] and [7], S_{ideal} is given by the Ernst equation describing the ideally spoiled steady-state signal (21):

$$S_{ideal} = K \cdot \frac{1-E_1}{1-E_1 \cdot \cos\alpha_i} \cdot \sin\alpha_i \quad \text{with} \quad E_1 := \exp(-TR/T_1) \quad [8]$$

The proportionality factor K, defined here as in Equations [1] and [2], cancels out in the ratio s_α. The nominal flip angle is corrected voxelwise to yield the actual value $\alpha_{act} = c_{B1} \cdot \alpha_{nom}$, whereas the B_1 scaling factor c_{B1} is either derived from Equation [4] or an external reference measurement. The flip angle and phase distributions across the slice (α_i and θ_i, i = {1, 2,…, N) are retrieved for the B_1-corrected flip angle α_{act} from the lookup table. Analogously to the calculation of c_{B1} described above, T_1 can be estimated based on the signal ratio s_α by means of a golden section search using an upper guess of $T_{1,u} = 10$ s:

$$T_1 = \arg\min\{T_1 \in [0, T_{1,u}]: |s_{\alpha,meas} - s_{\alpha,calc}(T_1)|\} \quad [9]$$

with $s_{\alpha,meas}$ referring to the measured signal ratio and $s_{\alpha,calc}$ denoting the calculated ratio derived from Equations [5] to [8].

In vitro and *in vivo* validation

The proposed simultaneous VFA B_1 and T_1 mapping was evaluated at 1.5 T and 3 T for the protocols specified above, i.e., 10 spiral interleaves with R = 1 at 1.5 T (acquisition time: 28 s) and 20 spiral interleaves with R = 1 / R = 2 at 3 T (acquisition time: 53 s / 28 s). At both field strengths, the method was validated *in vitro* in a manganese-doped aqueous probe (0.125 mM $MnCl_2$ in H_2O) with tissue-like T_1 and T_2 values as well as *in vivo* in the human brain of two healthy subjects (male, 30 y/o and female, 32 y/o) for white matter (WM) and gray matter (GM) characterization.

For validation purposes, reference values for the B_1 scaling factor (c_{B1}) were derived based on the vendor's product implementation for B_1 mapping; i.e., two fast 2D multislice gradient-echo acquisitions with and without a preconditioning RF pulse including a Turbo-FLASH readout (22,23). 3D median filtering was applied to the obtained B_1 maps with the same kernel sizes as used for the processing of the VFA B_1. The geometry and slice positioning of the reference measurement was exactly matched to one of the slice groups acquired by single-shot spiral imaging for multislice VFA B_1 mapping; number of acquired slices: 11, center-to-center slice spacing: 15 mm, resolution: 5.3 x 5.3 x 3 mm^3, total scan time: 12 s.

The *in vitro* agreement between the reference B_1 and the spiral VFA B_1 was analyzed after median filtering for the 11 matching slices by linear least-squares fitting of the data and the derivation of the intraclass correlation coefficient (ICC) (24). Additionally, Bland-Altman plots were calculated and the mean relative difference as well as the 95% limits of agreement were extracted from the data. The relative difference was derived in percentage as [(B_1 REF – B_1 Spiral VFA)/Mean B_1]·100 and the 95% limits of agreement were calculated as the mean relative difference ±1.96 times the standard deviation (SD) of the relative differences. For visualization of the correlation scatter and Bland-Altman plots, the underlying data was partitioned into 50 bins along each dimension and the normalized number of voxels in each bin was displayed by coloured density plots. The corresponding *in vitro* T_1 distributions were visualized by calculating histograms for a T_1 range from 200 to 1600 ms with a fixed bin size

of 2.5 ms. The histogram peaks were computed by a probability density estimation of the underlying T_1 distribution using the normal function as kernel smoother. The T_1 histogram peak values were compared to the reference T_1 obtained from six single-slice inversion-recovery turbo-spin-echo (IR-TSE) scans with variable inversion times TI = [100, 200, 400, 800, 1600, 3200] ms. Each of these scans took 2 min 50 s to complete, thus in total 17 min. The ability of the spiral VFA B_1 to correct transmit field inhomogeneities effectively for accurate T_1 mapping was assessed in comparison to the reference B_1 as well as to the case without any B_1 correction.

For the *in vivo* validation, the $S_{\beta 1}$ and $S_{\alpha 1}$ contrasts were registered to $S_{\beta 2}$ and $S_{\alpha 2}$ using the software packages FSL (25) and AFNI (26). The transformation matrix was calculated for the registration of the $S_{\alpha 1}$ to the $S_{\alpha 2}$ dataset and then applied to the $S_{\beta 1}$ dataset. Additionally, the $S_{\alpha 1}$ and $S_{\alpha 2}$ datasets were skull-stripped. The low-resolution $S_{\beta 1}$ and $S_{\beta 2}$ contrasts were interpolated to the size of $S_{\alpha 1}$ and $S_{\alpha 2}$. Because of the ultrashort scan times per slice group required for the acquisition of the $S_{\beta 1}$ and $S_{\beta 2}$ contrasts, i.e., 250 ms and 350 ms, respectively, the acquisition pairs $S_{\beta 1}$ and $S_{\alpha 1}$ as well as $S_{\beta 2}$ and $S_{\alpha 2}$ were considered to be intrinsically coregistered. The external B_1 reference scan was registered and interpolated to $S_{\alpha 2}$. After registration and interpolation, quantitative spiral VFA B_1 and T_1 maps were calculated based on the four acquired contrasts as described in the previous subsection. The obtained B_1 maps as well as the reference B_1 maps were median filtered and subsequently skull-stripped. The agreement between the two B_1 quantification methods was then assessed for whole-brain data in an analogous manner as for the *in vitro* data by linear least-squares fitting, the derivation of the ICC, as well as through a Bland-Altman analysis. For visualization of the correlation scatter and Bland-Altman plots, 75 bins were used along each dimension.

In vivo whole-brain T_1 histograms were calculated for a T_1 range from 200 to 3000 ms and a bin size of 2.5 ms. The distribution of whole-brain T_1 values was approximated using a Gaussian mixture model (GMM) with four components that was optimized for the 1.5 T and 3 T spiral VFA data acquired without parallel imaging acceleration (R = 1) and proved to reliably reflect the white as well as gray matter T_1 histogram peaks. The reproducibility of white and gray matter T_1 peak assessment based on the proposed VFA B_1 and T_1 mapping protocols was analyzed in a healthy volunteer (male, 30 y/o) that was measured 10 times at

both field strengths. The WM and GM T_1 histogram peaks were quantified by the mean of the corresponding fitted Gaussian component. In between consecutive scan sessions, the MR table was moved to the home position and the subject was repositioned to enforce new scan conditions (including frequency adjustment and shimming). At 3 T, one scan session included both investigated spiral VFA protocols, i.e., acquisitions without and with parallel imaging acceleration. The T_1 reproducibility was assessed quantitatively by calculating the coefficient of variation (given by the ratio of the standard deviation to the mean) for the fitted WM and GM T_1 peak values as well as voxelwise to visualize the reproducibility in local brain structures.

The *in vivo* VFA T_1 accuracy was assessed in a second healthy volunteer (female, 32 y/o) at 1.5 T and 3 T by comparison to the T_1 values obtained from gold standard single-slice IR-TSE scans at identical in-plane resolution and slice thickness with variable inversion times as specified above for the *in vitro* case. The positioning of the IR-TSE slice was matched to one of the central slices contained in the stack of 55 slices as acquired with the VFA protocol. On the matching slice, mean T_1 values were assessed for ROIs defined in frontal white matter (WM_1), occipital white matter (WM_2), and for gray matter in the putamen (GM_1) and the caudate nucleus head (GM_2). For each brain tissue structure (WM_1, WM_2, GM_1, GM_2), the selected ROI consisted of a subregion in the left and a subregion in the right hemisphere.

RESULTS

Excellent agreement between the spiral VFA B_1 and the reference B_1 is observed *in vitro* in a manganese-doped probe, as manifest from the linear fit that yielded slope values close to 1 for all three investigated protocols; concretely between 0.952 and 1.004 (cf. Fig. 2, left column). Correspondingly, high ICC values are found: 0.986 for the measurement at 1.5 T and 0.992 for the two protocols evaluated at 3 T (with R = 1 and R = 2). The Bland-Altman analysis (Fig. 2, right column) corroborates the strong agreement between the two B_1 mapping techniques as reflected by low mean relative differences and narrow 95% limits of agreement. At 1.5 T, a mean relative difference of 0.8% with 95% limits of agreement of ±1.8% is observed. At 3 T, mean relative differences of 0.8% and 1.1% for R = 1 and R = 2, respectively, with 95% limits of agreement of ±3.6% are found. Note that the parallel

imaging acceleration (R = 2) affects only the imaging module and not the preparation module used for B_1 mapping (cf. Fig. 1a).

Simultaneous spiral VFA B_1 and T_1 mapping yields narrow *in vitro* T_1 distributions with T_1 histogram peaks that agree well with the reference T_1 (cf. Fig. 3, top row). While the protocols at 1.5 T and 3 T without parallel imaging acceleration perform comparably, an acceleration factor of R = 2 at 3 T causes a slight broadening of the T_1 histograms because of the lower SNR, however, only marginally affecting the agreement with the reference T_1. The deviations of the T_1 peaks from the nominal reference value are 1.5 % at 1.5 T, 0.4 % at 3 T with R = 1, and 3.1 % at 3 T with R = 2. The reference B_1 yields similar T_1 results with somewhat reduced accuracy in comparison to the spiral VFA B_1 (cf. Fig. 3, middle row) as apparent from the slightly broader histograms and increased deviations of the T_1 histogram peaks from the reference T_1 value: 3.7 % at 1.5 T, 2.0 % at 3 T with R = 1, and 6.6 % at 3 T with R = 2. If B_1 inhomogeneities are not corrected, the corresponding histograms of the same data are highly degraded (cf. Fig. 3, bottom row), resulting in substantially broader T_1 distributions and a shift of the histogram T_1 peaks towards lower T_1 values, in particular for the scans at 3 T.

Similar to the *in vitro* data, the whole-brain validation of the spiral VFA B_1 against the reference B_1 yields excellent agreement between the two methods, as reflected by the linear fit characterized by slope values relatively close to 1, concretely 0.901 at 1.5 T and 0.934 / 0.945 at 3 T with R = 1 / R = 2, as well as the derived high ICC values. At 1.5 T, an ICC of 0.980 is found while at 3 T, an ICC of 0.987 is observed for both protocols, with R = 1 and R = 2, thus reflecting high conformity (cf. Fig. 4, left column). A slight overestimation of the spiral VFA B_1 in comparison to the reference B_1 can be seen as quantified by the Bland-Altman analysis (Fig. 4, right column). The Bland-Altman plots show a mean relative difference of -2.6% with 95% limits of agreement of ±2.1% at 1.5 T. At 3 T, mean relative differences of -3.6% and -3.7% with 95% limits of agreement of ±3.1% and ±3.2% are found for R = 1 and R = 2, respectively. Note that the accelerated parallel acquisition refers to the imaging module (cf. Fig. 1a). It is thus not expected to find noise impairment in the B_1 maps, in accordance with the results (cf. Figs. 2 and 4, middle row versus bottom row).

The B_1-corrected whole-brain T_1 histograms obtained with simultaneous spiral VFA B_1 and T_1 estimation at 1.5 T and 3 T without parallel imaging acceleration show clearly delineated

WM and GM T_1 peaks (cf. Fig. 5a, left and middle column). The acceleration with R = 2 at 3 T exhibits a similar T_1 histogram width compared to the unaccelerated measurement; however, the delineation of the WM and GM peaks appears slightly impaired (cf. Fig. 5a, right column). Recalculation of the same T_1 data without B_1 correction leads to a considerable broadening of the T_1 histograms, in particular at 3 T, accentuating the necessity for accurate B_1 mapping (cf. Fig. 5b).

The proposed simultaneous B_1 and T_1 mapping method is highly reproducible, as demonstrated by assessing the WM and GM T_1 whole-brain histogram peaks for 10 consecutive measurements of a healthy volunteer (cf. Fig. 6). The high reproducibility is corroborated by the low coefficients of variation that are found for the WM / GM peaks: 0.003 / 0.004 at 1.5 T, 0.004 / 0.007 at 3 T with R = 1, and 0.006 / 0.007 at 3 T with R = 2. Despite the lower SNR of the accelerated scan at 3 T, the found coefficient of variations are only slightly lower compared to the unaccelerated data. The mean assessed WM / GM T_1 histogram peaks agree well with literature values (27): 653 ± 2 ms / 1027 ± 4 ms at 1.5 T, 872 ± 3 ms / 1279 ± 9 ms at 3 T with R = 1, and 866 ± 5 ms / 1247 ± 9 ms at 3 T with R = 2. Consequently, only a marginal T_1 peak underestimation is observed for the accelerated relative to the unaccelerated measurement at 3 T. The voxelwise maps of the coefficient of variation reveal a consistently low T_1 variability in most brain tissue structures (cf. representative slice shown in Figure 7). Slightly increased variability can be observed in cortical gray matter in comparison to the surrounding tissue. It can be seen that the increased SNR at higher field strength (here 3 T) leads to a generally reduced voxelwise variability in comparison to 1.5 T. Furthermore, the standard deviation map corresponding to the accelerated protocol shows increased values compared to the unaccelerated measurement reflecting noise amplification associated with the parallel imaging acceleration.

The *in vivo* T_1 validation against the IR reference method demonstrates good agreement for the selected ROIs in WM and GM brain structures of a healthy volunteer (cf. Table 1). Overall, the relative deviation between the spiral VFA T_1 and the IR T_1 is $\lesssim$ 7% at both field strengths for all ROIs, except for the T_1 obtained in the caudate nucleus head (GM_2) at 3 T with the accelerated protocol (R = 2) where a relative deviation of $\approx$ 11% is observed.

In Figures 8 and 9, representative *in vivo* B_1 and T_1 maps derived from spiral VFA acquisitions in the human brain at 1.5 T and 3 T are shown. The obtained B_1 and T_1 maps appear free of spiral-related artifacts. Even though the B_1 shows clearly increased variations at 3 T, the corresponding T_1 maps exhibit a homogeneous contrast, thus indicating successful B_1 correction. The typical dependence of T_1 on the field strength is noticeable, i.e., larger T_1 values at higher fields. The obtained T_1 maps reveal WM and GM structures at clinically relevant resolution with good SNR (cf. Fig. 8). In Figure 9, the potential of the proposed technique to deliver simultaneous whole-brain B_1 and T_1 mapping at 1.5 T and 3 T in scan times shorter than one minute is demonstrated by displaying the coronal and sagittal views of the acquired 55 axial slices, covering the entire brain.

DISCUSSION

A simultaneous B_1 and T_1 mapping method was suggested based on the implementation of a steady-state prepared spiral multislice VFA acquisition scheme offering exceptionally short scan times – less than one minute for B_1-corrected whole-brain VFA T_1 quantification at 1.5 T and 3 T. No additional scan time is required for B_1 mapping since flip angle miscalibrations can be estimated in an ultrafast manner based on intrinsically coregistered contrasts acquired by a single-shot spiral readout during the steady-state preparation module (cf. Fig. 1a). The net acquisition time for the two contrasts required for B_1 mapping ($S_{\beta 1}$ and $S_{\beta 2}$) corresponds to the steady-state preparation time and equals only 3 s in total for the acquisition of five slice groups (i.e. 55 slices), covering the whole brain, at two different flip angles.

The volumes acquired at different flip angles were registered onto each other. Potential bulk head motion occurring between the acquisition of different slice groups was not considered. However, since the acquisition time per volume was rather short (14 s at 1.5 T with R = 1 / 3 T with R = 2 and 26.5 s at 3 T with R = 1), motion between slice groups was expected to be negligible for the performed measurements. For certain subject groups, e.g. children who may have difficulties to follow the instruction to lie still, additional correction of motion between slice groups may be needed.

In Ref. (13), it was demonstrated that spiral multislice VFA imaging in combination with an external B_1 reference scan achieves high T_1 accuracy for human brain tissue characterization at 1.5 T. In this work, spiral multislice VFA is translated to higher field strengths and results for 1.5 T and 3 T, the current clinical standards, are presented. As a result of the simultaneous B_1 estimation during the preparation module, the scan times could be shortened further with respect to the previous study (13). Excellent agreement between the novel spiral VFA B_1 and an acquired standard reference B_1 was found, both *in vitro* as well as *in vivo*. The generally high accuracy of the calculated VFA T_1 values is demonstrated by comparison against gold standard IR data in selected white and gray matter structures of a healthy volunteer. Residual deviation from the reference T_1 may be caused by residual errors in the derived B_1 values or by spatial misalignment of the ROIs since motion, occurring during the long acquisition times of the single-slice reference scans, cannot be corrected.

At 1.5 T, reliable whole-brain T_1 quantification was feasible based on the acquisition of 10 spiral interleaves within an overall scan time of only 28 s. At 3 T, the increased off-resonance effects, e.g., at air-tissue interfaces, necessitated an increase of the acquired spiral interleaves from 10 to 20 to reduce the readout time and thus off-resonance sensitivity. The increased number of spiral interleaves came along with prolonged scan times, yielding 53 s for whole-brain coverage. To achieve scan times identical to the measurements at 1.5 T, a second protocol was investigated at 3 T consisting of 20 spiral interleaves combined with a SPIRiT acceleration factor of R = 2, shortening the acquisition time to 28 s. Both protocols demonstrated ability to deliver high-quality whole-brain T_1 maps at 3 T without any visible image degradations (cf. Figs. 8 and 9). The lower SNR of the accelerated protocol resulted in a broader T_1 distribution (observed both *in vitro* as well as *in vivo*), which, however, generally only marginally affected the T_1 accuracy with respect to the unaccelerated data.

The reproducibility of T_1 values assessed from 10 consecutive measurements of a healthy volunteer was overall high for human brain tissues. However, a slightly increased variability in cortical gray matter was observed in the voxelwise maps of the coefficient of variation (cf. Fig. 7). Since cortical gray matter consists of thin layers, the higher variability can likely be attributed to registration misalignment or to partial volume effects related to the proximity to cavities filled with cerebrospinal fluid (CSF). Regions of increased standard deviations can be observed for the accelerated protocol at 3 T. The g-factor associated with the parallel imaging acceleration may cause locally varying noise enhancement and may vary across

subjects. The increased relative deviation from the T_1 reference measurement of ~11% observed in the caudate nucleus head for the accelerated protocol may thus possibly arise from a combination of partial volume effects near the ventricles and g-factor related noise enhancement (cf. Table 1, GM_2).

It has to be noted that this work exploits the speed limit of spiral multislice VFA. A further acceleration may hardly be possible with the proposed scheme as shorter scan times lead to non-steady-state conditions that are expected to reduce the accuracy of tissue T_1 quantification and more importantly, can lead to artifacts related to the extremely long T_1 relaxation times of CSF, in particular for the high-flip-angle acquisitions (cf. Ref. (13)). Furthermore, since the preparation module is optimized to effectively place tissues into steady state, accurate T_1 quantification of CSF is not feasible with the investigated protocol (13). In addition, CSF exhibits clearly increased T_1 variability (cf. Fig. 7) compared to tissue likely caused by physiological motion.

The proposed VFA acquisition scheme demonstrated ability to intrinsically eliminate the two main error sources in VFA-based tissue T_1 quantification: residual T_2 dependency caused by incomplete spoiling and B_1 inhomogeneities. The spoiling efficiency of the used 2D multislice sequence is extremely high because of the combined long-TR and diffusion spoiling (cf. 'Methods' section) such that residual transverse coherences are expected to be completely eliminated. A single-shot spiral readout during the preparation module enables simultaneous ultrafast B_1 mapping and as a result accurate T_1 mapping with high reproducibility, manifest from the results presented in this work.

CONCLUSION

Based on a steady-state prepared spiral multislice VFA imaging scheme, simultaneous B_1 and T_1 mapping proved to be reliable and highly reproducible in the human brain at 1.5 T and 3 T. The proposed protocol offered the acquisition of 55 slices providing whole-brain coverage at clinically relevant resolution (1.3 x 1.3 x 3 mm^3) in less than one minute; concretely 28 s / 53 s at 1.5 T / 3 T without parallel imaging acceleration and 28 s at 3 T with a SPIRiT acceleration factor of 2. The fast acquisition, volumetric coverage, and high accuracy for

tissue T_1 characterization accentuate the potential of the presented technique to be applied in clinical settings where snapshot-like whole-brain T_1 mapping is needed.

ACKNOWLEDGEMENT

This work was supported by a grant from the Swiss National Science Foundation (SNF 325230-153332).

REFERENCES

1. Tofts P. Quantitative MRI of the Brain. Chichester: John Wiley & Sons Ltd; 2003.
2. Drain LE. A direct method of measuring nuclear spin-lattice relaxation times. P Phys Soc Lond A 1949;62(353):301-306.
3. Hahn EL. An accurate nuclear magnetic resonance method for measuring spin-lattice relaxation times. Physical Review 1949;76(1):145-146.
4. Look DC, Locker DR. Time saving in measurement of NMR and EPR relaxation times. Rev Sci Instrum 1970;41:250-251.
5. Brix G, Schad LR, Deimling M, Lorenz WJ. Fast and precise T1 imaging using a TOMROP sequence. Magn Reson Imaging 1990;8(4):351-356.
6. Fram EK, Herfkens RJ, Johnson GA, Glover GH, Karis JP, Shimakawa A, Perkins TG, Pelc NJ. Rapid calculation of T1 using variable flip angle gradient refocused imaging. Magn Reson Imaging 1987;5(3):201-208.
7. Stikov N, Boudreau M, Levesque IR, Tardif CL, Barral JK, Pike GB. On the accuracy of T1 mapping: Searching for common ground. Magn Reson Med 2014.
8. Barral JK, Gudmundson E, Stikov N, Etezadi-Amoli M, Stoica P, Nishimura DG. A robust methodology for in vivo T1 mapping. Magn Reson Med 2010;64(4):1057-1067.
9. Henderson E, McKinnon G, Lee TY, Rutt BK. A fast 3D Look-Locker method for volumetric T1 mapping. Magnetic Resonance Imaging 1999;17(8):1163-1171.
10. Deoni SC, Peters TM, Rutt BK. High-resolution T1 and T2 mapping of the brain in a clinically acceptable time with DESPOT1 and DESPOT2. Magn Reson Med 2005;53(1):237-241.
11. Yarnykh VL. Optimal radiofrequency and gradient spoiling for improved accuracy of T1 and B1 measurements using fast steady-state techniques. Magn Reson Med 2010;63(6):1610-1626.
12. Heule R, Bieri O. Rapid and robust variable flip angle T1 mapping using interleaved two-dimensional multislice spoiled gradient echo imaging. Magn Reson Med 2017;77(4):1606-1611.
13. Heule R, Pfeuffer J, Bieri O. Snapshot whole-brain T1 relaxometry using steady-state prepared spiral multislice variable flip angle imaging. Magn Reson Med 2018;79(2):856-866.

14. Preibisch C, Deichmann R. Influence of RF spoiling on the stability and accuracy of T1 mapping based on spoiled FLASH with varying flip angles. Magn Reson Med 2009;61(1):125-135.
15. Meyer CH, Zhao L, Lustig M, Jilwan-Nicolas M, Wintermark M, Mugler JP, Epstein FH. Dual-density and parallel spiral ASL for motion artifact reduction. Proceedings ISMRM 2011. p 3986.
16. Lustig M, Pauly JM. SPIRiT: Iterative self-consistent parallel imaging reconstruction from arbitrary k-space. Magn Reson Med 2010;64(2):457-471.
17. Tan H, Meyer CH. Estimation of k-space trajectories in spiral MRI. Magn Reson Med 2009;61(6):1396-1404.
18. Ernst RR, Bodenhausen G, Wokaun A. Principles of Nuclear Magnetic Resonance in One and Two Dimensions. Oxford: Clarendon Press; 1987.
19. Press WH, Teukolsky SA, Vetterling WT, Flannery BP. Numerical Recipes: The Art of Scientific Computing. Cambridge: Cambridge University Press; 2007.
20. Parker GJ, Barker GJ, Tofts PS. Accurate multislice gradient echo T1 measurement in the presence of non-ideal RF pulse shape and RF field nonuniformity. Magn Reson Med 2001;45(5):838-845.
21. Bernstein MA, King KF, Zhou XJ. Handbook of MRI Pulse Sequences. Burlington, MA: Elsevier Academic Press; 2004.
22. Fautz HP, Vogel M, Gross P, Kerr A, Zhu Y. B1 mapping of coil arrays for parallel transmission. Proceedings ISMRM 2008. p 1247.
23. Chung S, Kim D, Breton E, Axel L. Rapid B1+ mapping using a preconditioning RF pulse with TurboFLASH readout. Magn Reson Med 2010;64(2):439-446.
24. Shrout PE, Fleiss JL. Intraclass correlations: uses in assessing rater reliability. Psychol Bull 1979;86(2):420-428.
25. Smith SM, Jenkinson M, Woolrich MW, Beckmann CF, Behrens TEJ, Johansen-Berg H, Bannister PR, De Luca M, Drobnjak I, Flitney DE, Niazy RK, Saunders J, Vickers J, Zhang YY, De Stefano N, Brady JM, Matthews PM. Advances in functional and structural MR image analysis and implementation as FSL. Neuroimage 2004;23:S208-S219.
26. Cox RW. AFNI: software for analysis and visualization of functional magnetic resonance neuroimages. Computers and biomedical research, an international journal 1996;29(3):162-173.

27. Rooney WD, Johnson G, Li X, Cohen ER, Kim SG, Ugurbil K, Springer CS, Jr. Magnetic field and tissue dependencies of human brain longitudinal 1H2O relaxation in vivo. Magn Reson Med 2007;57(2):308-318.

TABLE

T_1 in [ms]	1.5 T		3 T		
	Spiral VFA R = 1	IR-TSE	Spiral VFA R = 1	Spiral VFA R = 2	IR-TSE
White matter					
WM_1	609 ± 39	647 ± 14	850 ± 27	829 ± 59	863 ± 25
WM_2	620 ± 33	667 ± 22	819 ± 41	847 ± 55	873 ± 28
Gray matter					
GM_1	863 ± 71	922 ± 48	1179 ± 72	1214 ± 119	1200 ± 61
GM_2	1052 ± 105	1051 ± 60	1349 ± 92	1497 ± 113	1345 ± 66

Table 1. *In vivo* comparison of the T_1 values obtained from the proposed simultaneous spiral VFA B_1 and T_1 mapping to the derived gold standard IR-TSE T_1 values in the brain of a healthy volunteer measured at 1.5 T and 3 T. Mean T_1 values are reported for selected regions of interest in white and gray matter (cf. “Methods” section).

FIGURES

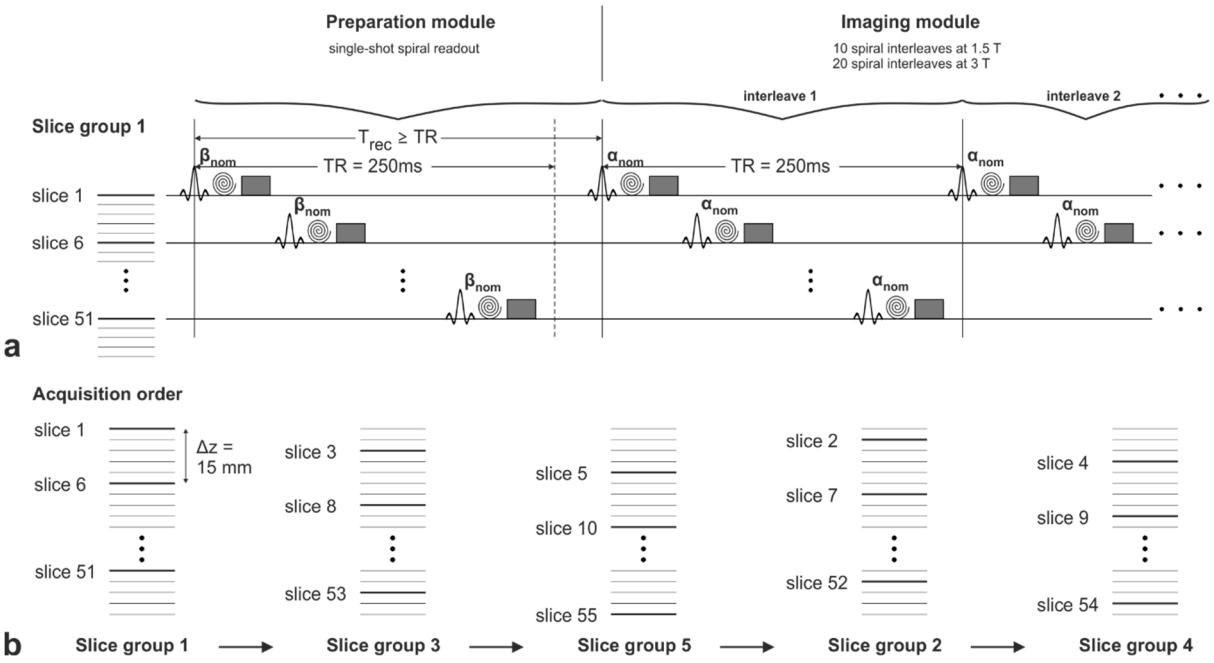

Figure 1. (**a**) Spiral 2D multislice VFA sequence diagram for the acquisition of one slice group. The approach to steady state is minimized by a preparation module consisting of a single slice-selective preparation pulse with flip angle β_{nom} and the FID signal is acquired by a single-shot 2D spiral readout. Following a recovery period T_{rec} (≥ TR), the imaging module consisting of a train of excitation pulses with flip angle α_{nom} starts. The time interval between the successive excitation of a given slice (= TR) is set to 250 ms. A total of 11 slices defining one slice group are excited within each TR and 10 / 20 spiral interleaves are acquired at 1.5 T / 3 T to encode the image. A large total net spoiler gradient moment is accumulated within TR due to the excitation of multiple slices: A_G = 459 (mT/m)·ms (≈ 11 · 41.7 (mT/m)·ms). The gray boxes indicate the spoiler gradients associated with the individual acquired slices. (**b**) To obtain whole-brain coverage, five different slice groups, each consisting of 11 slices separated by a center-to-center spacing of 15 mm (i.e., five times the slice thickness), are acquired consecutively with adapted positioning. The chosen slice group acquisition order ensures that the slices of consecutively measured groups are not adjacent to avoid slice crosstalk issues. Please note that the slice groups are labeled according to the anatomical position of the slice excited first within the group; leading to the following interleaved acquisition order: slice group 1 – 3 – 5 – 2 – 4.

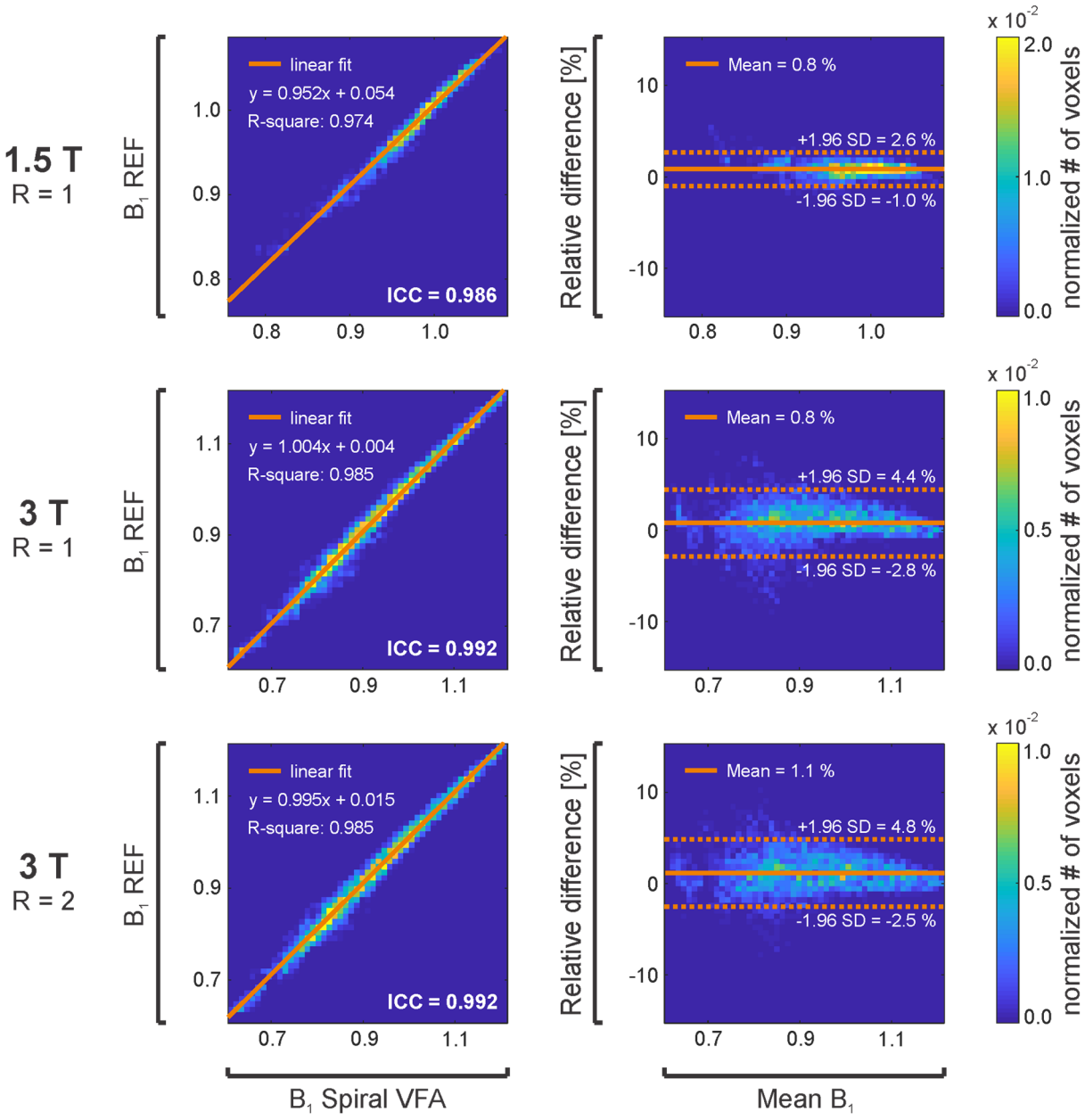

Figure 2. *In vitro* B_1 validation. Left column: binned scatter plots illustrating the correlation between the B_1 scaling factor c_{B1} obtained with spiral VFA (x-axis) and the reference method (y-axis) at 1.5 T (R = 1, top row) as well as at 3 T without (R = 1, middle row) and with (R = 2, bottom row) parallel imaging acceleration. The results from the linear least-squares fitting (solid orange line) and the calculated intraclass correlation coefficient are displayed. Right column: corresponding binned Bland-Altman plots quantifying the mean of the relative differences in percentage (solid orange line) and the 95% limits of agreement (dashed orange lines).

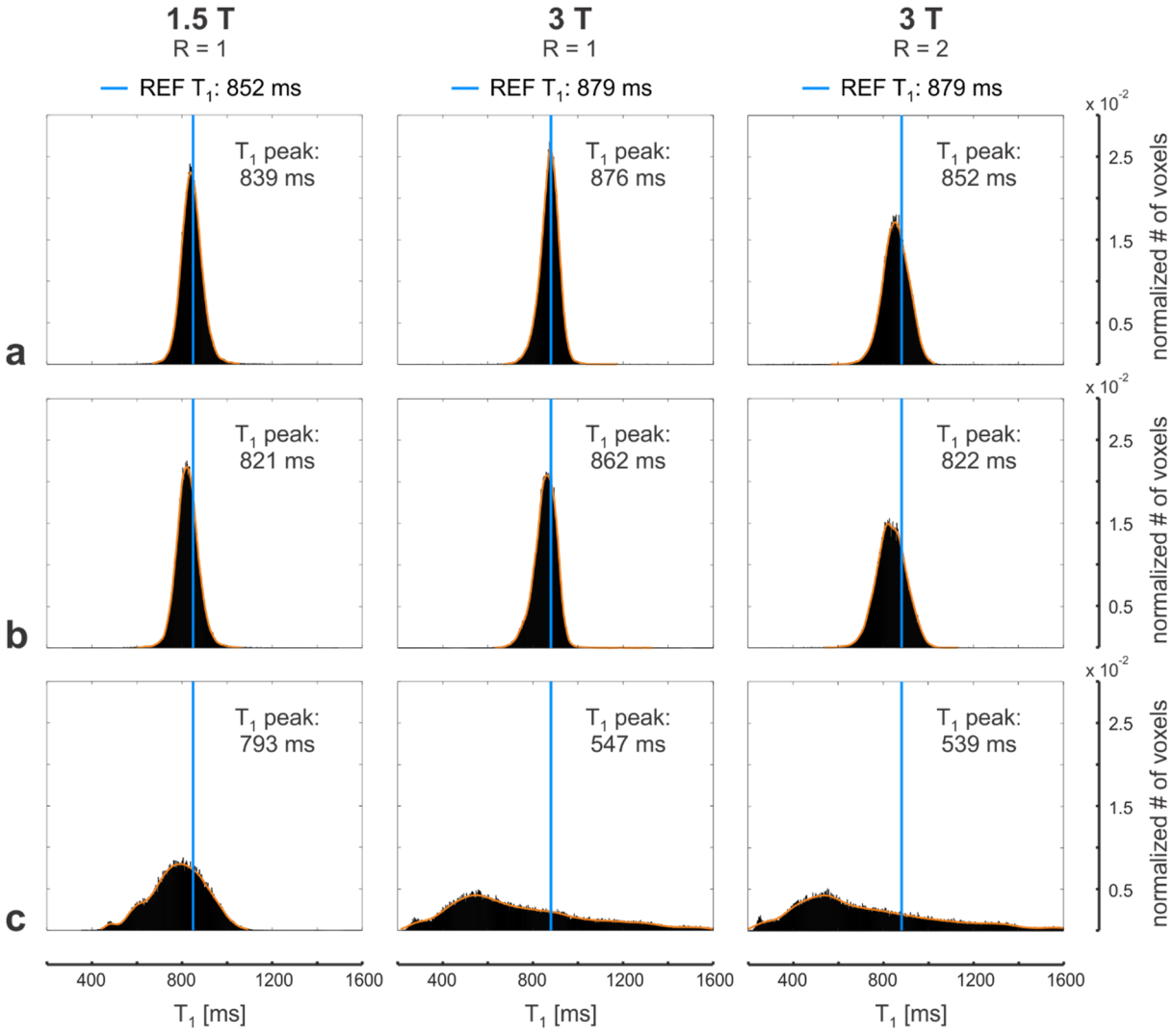

Figure 3. *In vitro* T_1 histograms obtained without parallel imaging acceleration at 1.5 T (left) and 3 T (middle) as well as with an acceleration factor of R = 2 at 3 T (right). The T_1 histogram peak values are computed based on probability density estimation using the normal distribution as kernel function (orange curve). The location of the reference T_1 value derived from the single-slice IR reference method is indicated by the vertical blue line. Flip angle miscalibrations are corrected by simultaneous B_1 determination based on a single-shot spiral readout during the preparation module (**a**) and by an external standard reference B_1 mapping method (**b**). For comparison, in (**c**), the same T_1 data are shown without any transmit field inhomogeneity correction.

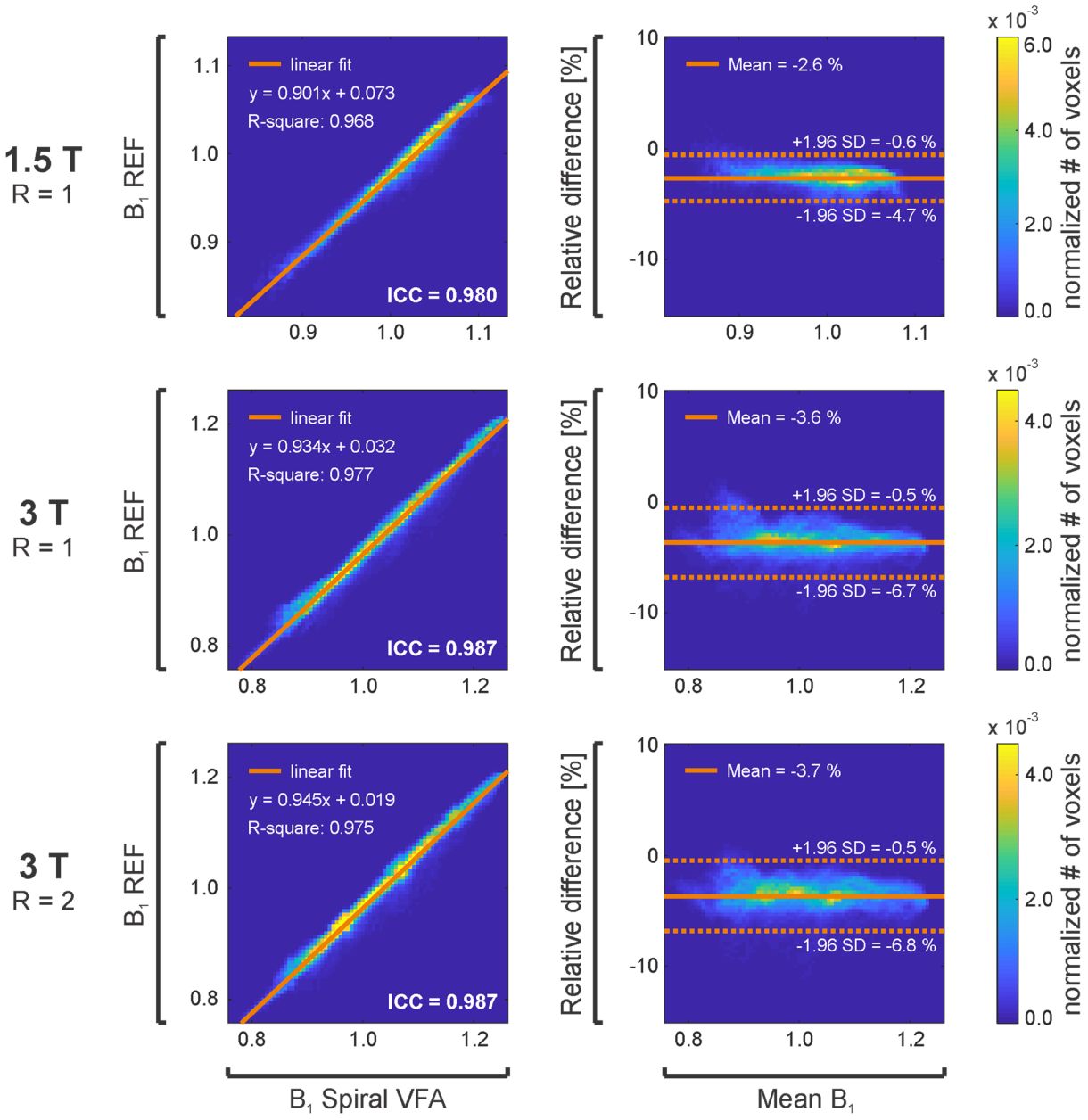

Figure 4. *In vivo* B_1 validation. Left column: binned B_1 scaling factor (c_{B1}) correlation plots of the spiral VFA B_1 (x-axis) and the reference B_1 (y-axis) obtained for representative whole-brain data acquired in the same healthy volunteer at 1.5 T (R = 1, top row) as well as at 3 T without (R = 1, middle row) and with (R = 2, bottom row) parallel imaging acceleration. Linear least-squares analysis is performed (solid orange line) and the intraclass correlation coefficient calculated to quantify the agreement between the two methods. Right column: corresponding binned Bland-Altman plots. The horizontal lines represent the mean of the relative differences in percentage (solid, orange) and the 95% limits of agreement (dashed, orange).

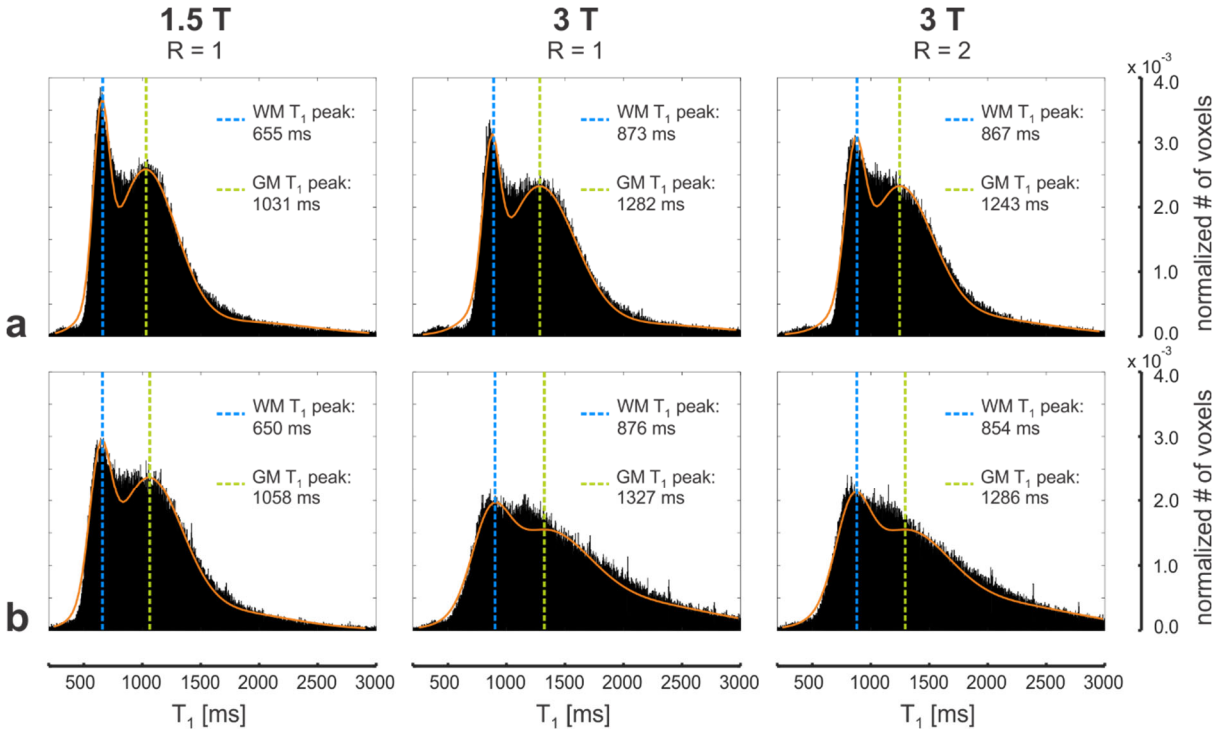

Figure 5. (**a**) Representative whole-brain T_1 histograms of a healthy volunteer derived from simultaneous spiral VFA B_1 and T_1 quantification without parallel imaging acceleration at 1.5 T (left) and 3 T (middle) as well as with an acceleration factor of R = 2 at 3 T (right). The WM peak (left blue line) and GM peak (right green line) values are assessed by fitting a Gaussian mixture model (GMM) to the data (orange curve). (**b**) For reference, the T_1 data shown in (a) is recalculated without correction of flip angle miscalibrations and the corresponding T_1 histograms including the GMM fit are displayed.

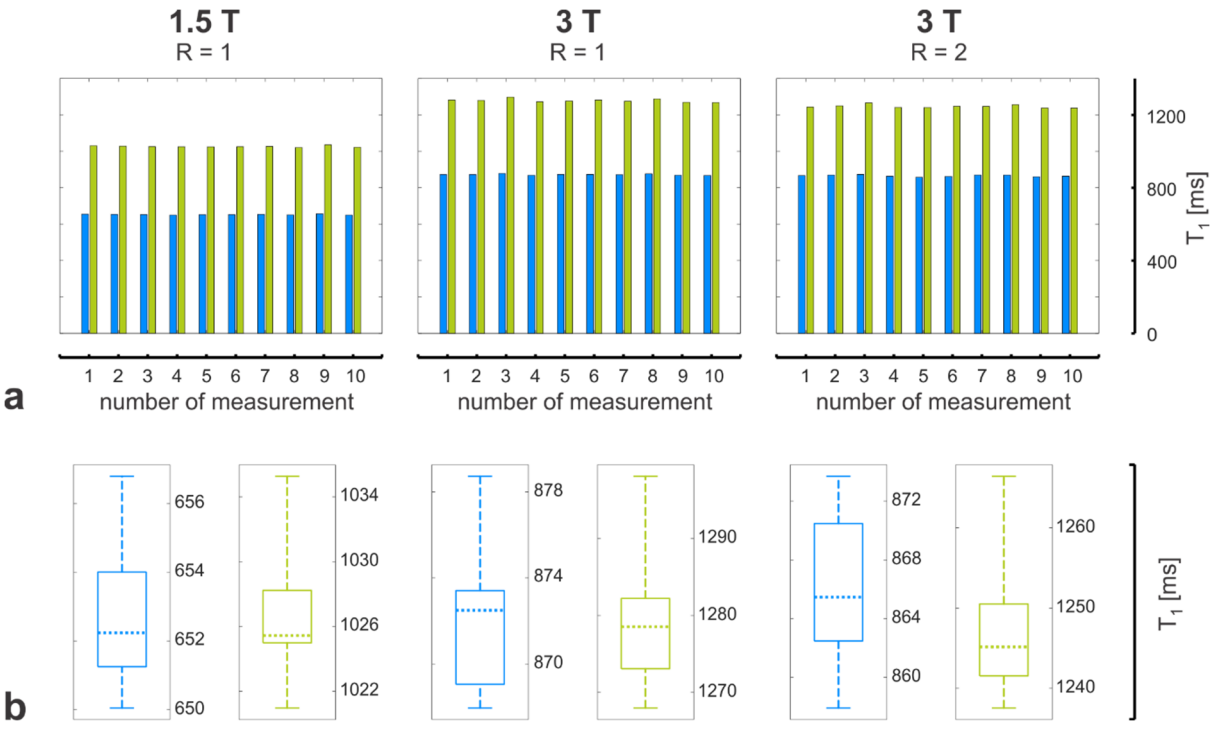

Figure 6. (**a**) Reproducibility analysis of simultaneous whole-brain VFA T_1 and B_1 mapping, assessed by the WM (blue bars) and GM (green bars) T_1 histogram peaks that were calculated from 10 consecutive measurements of a healthy volunteer at 1.5 T with R = 1 (left column) as well as at 3 T with R = 1 (middle column) and R = 2 (right column). (**b**) The corresponding box plots of the WM (left, blue) and GM (right, green) data shown in (a). The horizontal dotted lines represent the median T_1 histogram peak values, the bottom and top of the box refer to the lower and upper quartile values, respectively, and the vertical dashed lines indicate the extent of the data from minimal to maximal values.

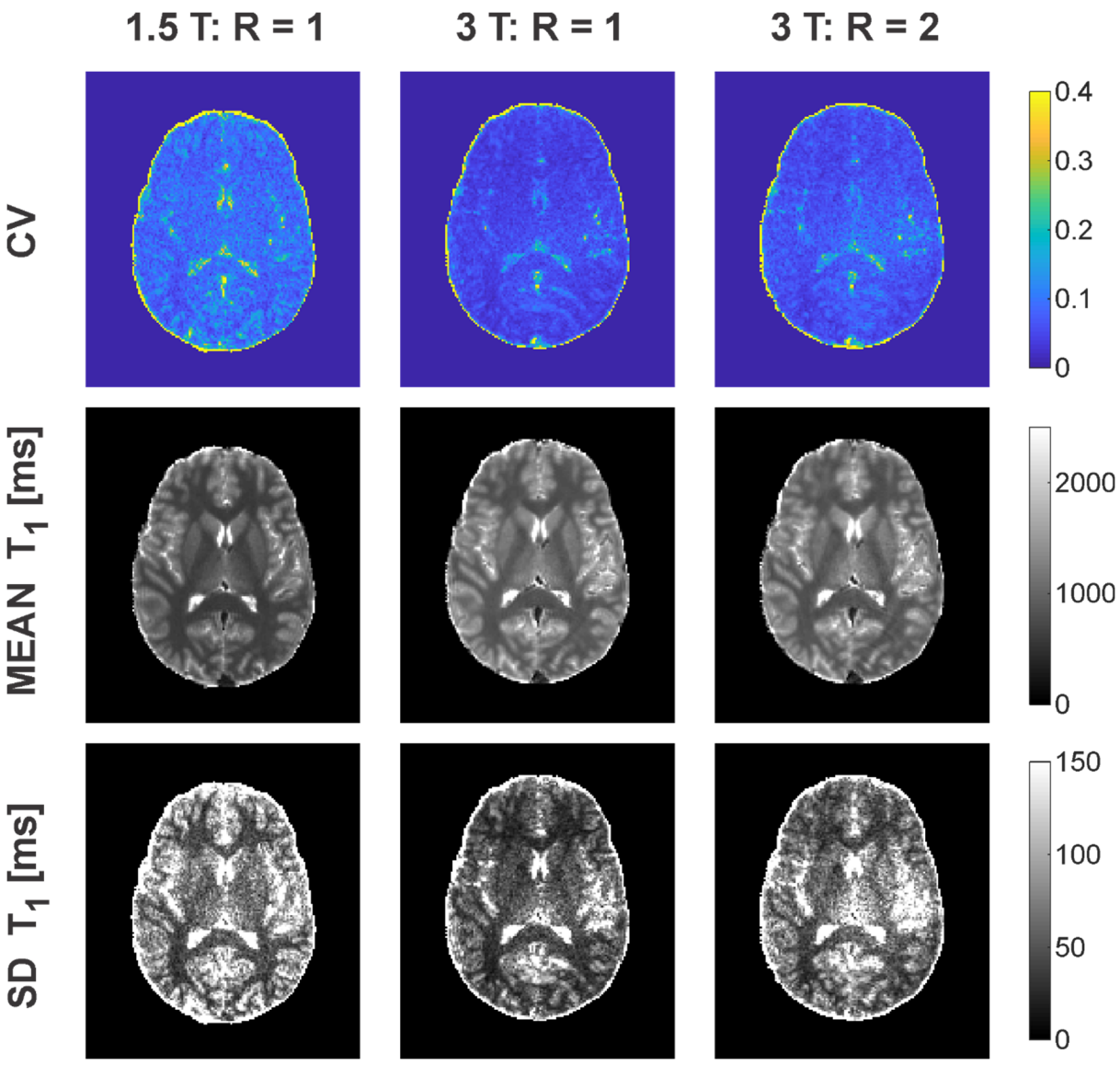

Figure 7. Top row: representative maps of the T_1 variability derived from a voxelwise calculation of the coefficient of variation (CV ≡ standard deviation (SD) / mean) for a healthy volunteer who was measured 10 times consecutively. Middle and bottom row: the corresponding mean T_1 and the standard deviation of the mean in each voxel, respectively. Left / middle / right column: 1.5 T with R = 1 / 3 T with R = 1 / 3 T with R = 2.

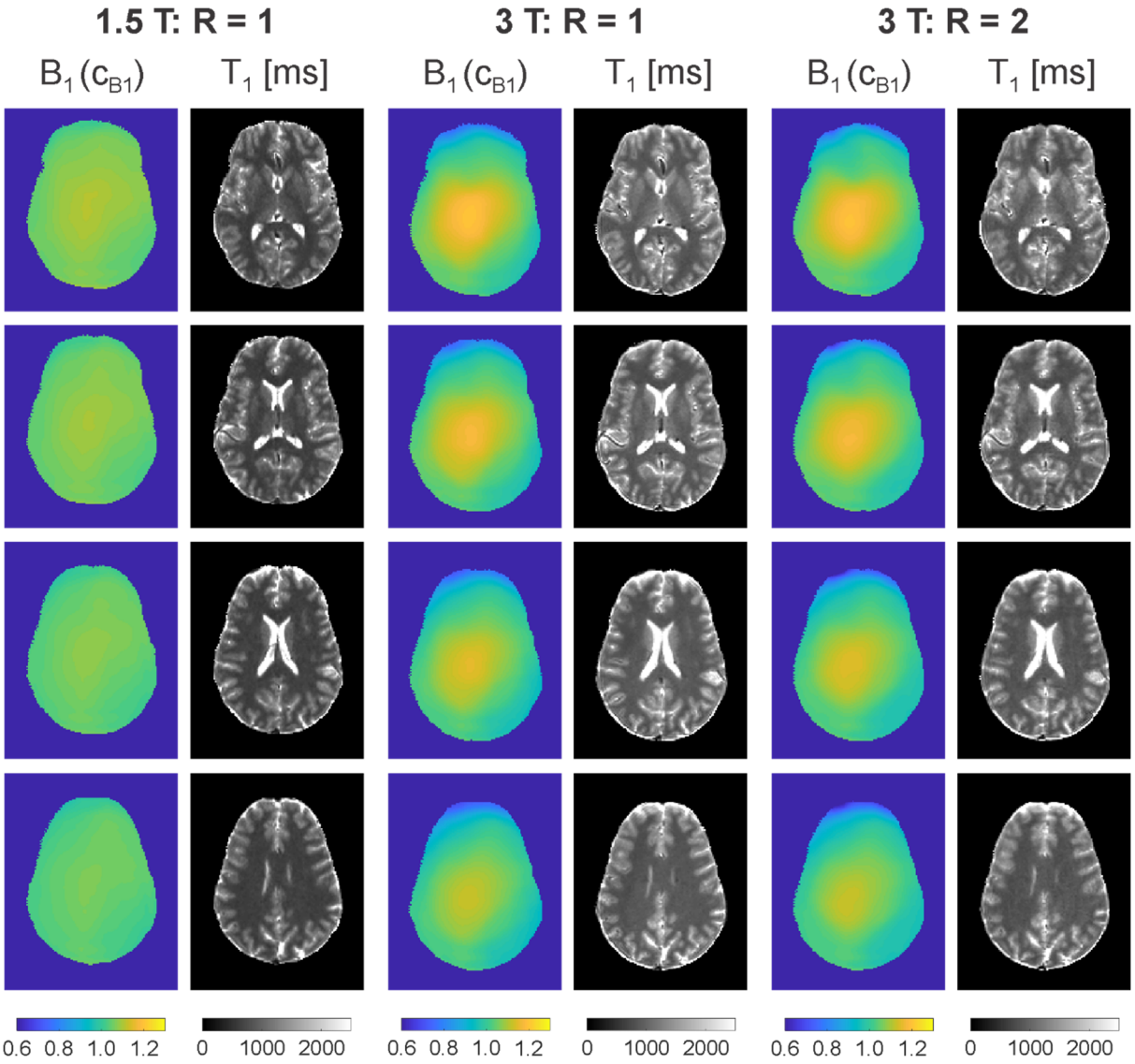

Figure 8. Representative *in vivo* B_1 (i.e., $c_{B1} = \alpha_{act} / \alpha_{nom}$) and T_1 maps obtained in the brain of a healthy volunteer at 1.5 T with R = 1 (left), at 3 T with R = 1 (middle), and at 3 T with R = 2 (right) based on spiral 2D multislice VFA acquisitions. The same scaling is used for the 1.5 T and 3 T data to show the field dependence of B_1 and T_1. Note that the 1.5 T and 3 T measurements are not registered onto each other but similar slices are selected. Four selected slices contained in the stack of in total 55 acquired axial slices are shown.

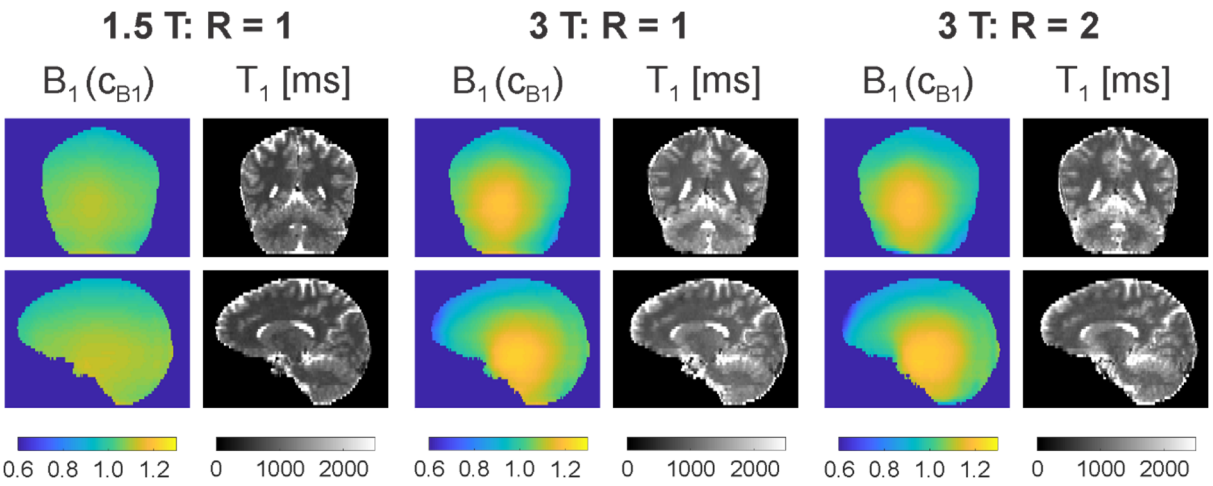

Figure 9. Coronal and sagittal views of the *in vivo* brain B_1 (c_{B1}) and T_1 maps corresponding to the datasets shown in Figure 8 and demonstrating whole-brain coverage. Left: measurement at 1.5 T with R = 1 completed in 28 s, middle: measurement at 3 T with R = 1 completed in 53 s, and right: measurement at 3 T with R = 2 completed in 28 s.